

Design of Iron Coordination Complexes as Highly Active Homogenous Water Oxidation Catalysts by Deuteration of Oxidation Sensitive Sites

Zoel Codolà,^[a] Ilaria Gamba,^[a] Ferran Acuña-Parés,^[b] Carla Casadevall,^[b] Martin Clémancey,^[d] Jean-Marc Latour,^[d] Josep María Lluís,^[a] Julio Lloret-Fillol,^{*,[b],[c]}
Miquel Costas^{*,[a]}

- a) Institut de Química Computacional i Catàlisi (IQCC) and Departament de Química, Universitat de Girona. Campus Montilivi; E17071 Girona, Catalonia (Spain)
miquel.costas@udg.edu
- b) Institute of Chemical Research of Catalonia (ICIQ), the Barcelona Institute of Science and Technology, Avinguda Paisos Catalans 16, 43007, Tarragona (Catalonia, Spain).
jlloret@iciq.es
- c) Catalan Institution for Research and Advanced Studies (ICREA), Passeig Lluís Companys, 23, 08010, Barcelona (Spain).
- d) Université Grenoble Alpes, CEA, CNRS, LCBM, pmb, F-38000 Grenoble, France

ABSTRACT

The nature of the oxidizing species in water oxidation reactions with chemical oxidants (CAN and NaIO₄), catalyzed by the pair of complexes α -[Fe(OTf)₂(mcp)] (mcp = *N,N'*-dimethyl-*N,N'*-bis(pyridin-2-ylmethyl)cyclohexane-1,2-diamine, OTf = trifluoromethanesulfonate anion), (**1 α**) and β -[Fe(OTf)₂(mcp)], (**1 β**) has been investigated. Mössbauer spectroscopy provides definitive evidence that **1 α** and **1 β** generate oxoiron(IV) species α -[Fe^{IV}(O)(OH₂)(mcp)]²⁺, (**2 α**) and β -[Fe^{IV}(O)(OH₂)(mcp)], (**2 β**) respectively, as the resting state, as early proposed on the basis of UV-Vis, resonance Raman and mass-spectrometry. Decomposition paths of the catalysts under experimental conditions of relevance to water oxidation catalysis have been investigated by identifying and quantifying ligand fragments that form upon catalyst degradation. This analysis correlates the water oxidation activity of **1 α** and **1 β** with stability against oxidative damage of the ligand *via* aliphatic C-H oxidation. The site of degradation and the relative stability against oxidative degradation is shown to be dependent on the topology of the catalyst. Furthermore, the mechanisms of catalyst degradation have been rationalized by computational analyses, which also explain why the topology of the catalyst enforces different oxidation sensitive sites. This information has served as the basis for creating a novel family of catalysts where sensitive C-H bonds have been replaced by C-D bonds. Consequently, deuterated analogs, D₄- α -[Fe(OTf)₂(mcp)] (**D₄-1 α**) and D₄- β -[Fe(OTf)₂(mcp)] (**D₄-1 β**), in which pseudobenzyl methylenic positions have been deuterated, and D₆- β -[Fe(OTf)₂(mcp)] (**D₆-1 β**), where NMe groups are deuterated, were prepared. The catalytic activity of the deuterated analogs has been studied using CAN as terminal oxidant. **D₄-1 α** proves to be an extraordinarily active and efficient catalyst (up to 91% of O₂ yield); it exhibits initial reaction rates identical to its protio analogue, but it is substantially more robust towards oxidative degradation and yields up to 2700 TON (n(O₂)/n(Fe)), which constitutes the highest value described for a first row transition metal catalyst. Altogether evidence that the water oxidation catalytic activity is performed by a well-defined coordination complex and not by iron oxides formed after oxidative degradation of the ligands.

INTRODUCTION

Water oxidation (WO) is one of the key components of natural photosynthesis and is regarded as one of the most challenging reactions to be mastered towards the development of an artificial version. The reaction is also of particular interest from a fundamental perspective because of its multi-electron and proton nature. Elucidation of the chemical aspects that govern the formation and lysis of the O-O bond, and the nature of the species involved in this reaction have also interesting derivations in the fields of oxidation catalysis and bioinorganic chemistry. Mechanistic understanding of WO reactions very much benefits from the study of molecular catalysts that operate under homogeneous conditions.¹⁻³ However, proving the nature of the catalytic species is often a non-trivial question.⁴⁻⁷ WO reactions involve highly oxidizing species that compromise the stability of molecular catalysts *via* oxidative damage. This issue is especially important in the case of coordination compounds and organometallic complexes bearing organic ligands.⁷⁻¹⁰ Oxidation of the precatalysts may produce novel discrete complexes that can be also active catalysts under homogeneous conditions. However, in a number of cases, initial oxidation of the molecular precatalysts can result in the formation of metal-oxide(hydroxide) nanoparticles, which may be also active WO catalysts. In some cases, WO may occur via parallel paths originating from molecular catalysts operating in a homogeneous regime, and metal-oxide nanoparticles that act as heterogeneous catalysts. In these cases, elucidation of the active species becomes very complicated.

Homogeneous and heterogeneous catalysts for WO based in first row transition metal (FRTM) ions attract major interest because of the earth abundant nature of these metals, which makes them potentially suitable for use in large scale.¹¹⁻¹⁵ Furthermore, the decisive role of Mn in the oxygen evolving complex (OEC) of PSII highlights the viability of the WO reaction at relatively complex, potentially labile and fragile structures based in FRTM ions. In a general sense, WO at manganese centers has served as general inspiration for catalyst design. Nevertheless, FRTM complexes are generally believed to be particularly sensitive to the oxidative and usually acidic conditions operating in water oxidation reactions. The usually labile nature of metal-ligand bonds for this class of compounds is believed to critically undermine their ability to act as long lasting WO catalysts, and there is a rich and lively debate on the exact nature of the species

responsible for the catalytic activity. Iron coordination complexes based on aminopyridine ligands have been explored as WO catalysts employing chemical, electrochemical and photochemical conditions.¹⁶⁻³⁵ Studies described so far have shown that the nature of the active species appears to be dependent on the nature of the catalysts, the oxidant and also the reaction conditions. The pair of catalysts α -[Fe(OTf)₂(mcp)] (mcp = *N,N'*-dimethyl-*N,N'*-bis(pyridin-2-ylmethyl)cyclohexane-1,2-diamine, OTf = trifluoromethanesulfonate anion), (**1 α**) and β -[Fe(OTf)₂(mcp)], (**1 β**) are interesting because being topological isomers, they exhibit very important differences in their catalytic activity.^{16,18} **1 α** is a particularly efficient WO catalyst when employing chemical oxidants such as cerium ammonium nitrate (CAN) and NaIO₄ under acidic conditions, but it rapidly degrades under photochemical and or basic conditions.^{16,20} In acidic aqueous solution, in the absence of an oxidant, it also undergoes slow hydrolytic decomposition, a behavior that can be traced to the lability of the high spin ferrous center.³⁶ On the other hand, the isomerically related **1 β** is poorly active with chemical oxidants and it is very rapidly degraded under acidic conditions.

The reaction mechanism proposed for these catalysts operating in acidic media with chemical oxidants such as CAN is shown in figure 1 and entails subsequent oxidation of the ferrous complexes, forming Fe^{IV}(O) species which constitute the resting state during catalysis.^{17,37} Reaction with Ce^{IV} generates a Fe^{IV}-O-Ce^{IV} complex, which has been spectroscopically characterized by a combination of UV-Vis, resonance Raman and high resolution mass-spectrometry (HRMS).¹⁶ These species can be regarded as an inner-sphere electron transfer (ET) intermediate in the path towards the 1e⁻ oxidation of the iron center. Thus, it evolves into the formation of a highly electrophilic Fe^V(O)(OH) reactive species and Ce^{III}. Computational analyses indicate that Fe^V(O)(OH) oxidizes the water molecule *via* a nucleophilic attack of the later over the terminal oxo ligand, assisted by an initial coordination of the reactive water molecule to the *cis*-hydroxide ligand.^{37,38}

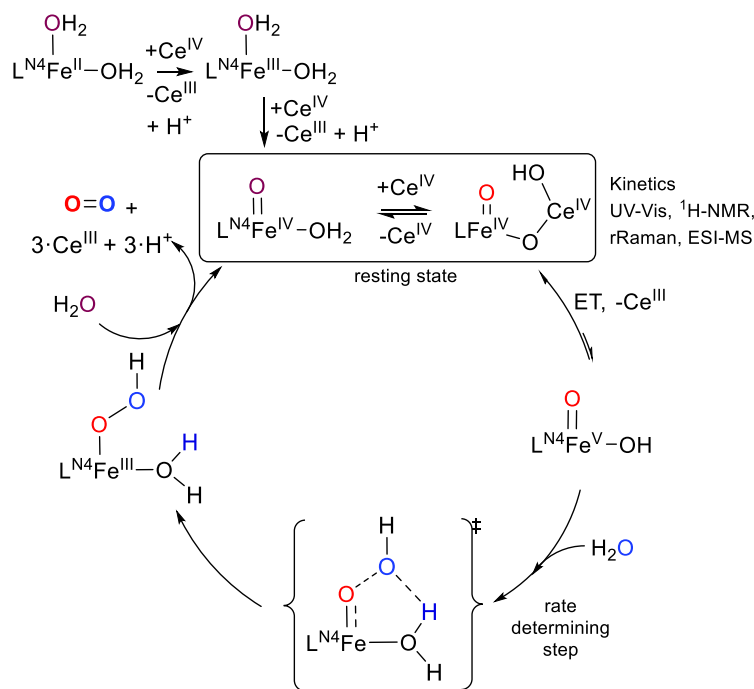


Figure 1. Reaction mechanism proposed for iron aminopyridine complexes operating in acidic media with chemical oxidants such as CAN.¹⁶

Despite there is a body of experimental evidence that supports this mechanistic proposal,¹⁶ the molecular nature of the catalysts has been questioned on the basis of the observation that structurally related iron complexes undergo rapid decomposition.³⁹ Furthermore, Mössbauer analysis that could provide unambiguous evidence for the formation of high valent iron oxo species in any molecular catalyst has not been described so far. In this scenario, establishing the nature of the catalyst resting state and comprehension of the nature of the deactivation processes can provide definitive evidence for the molecular nature of the catalysts, but also can provide clues to rationally design novel generations exhibiting improved activity.

With these considerations in mind, in this work we have characterized by Mössbauer spectroscopy the resting state of the catalysts **1α** and **1β** in water oxidation reactions with chemical oxidants, and we have studied their decay paths by a combination of experimental and computational methods. Ligand oxidation sensitive sites have been identified. This knowledge has served to design extraordinarily robust catalysts by deuteration of these sites, overall providing compelling evidence that WO under these

conditions takes place *via* molecular, high valent oxo-iron species. We envision that the current methodology may serve as a general strategy to prove the molecular nature of oxidation catalysts.

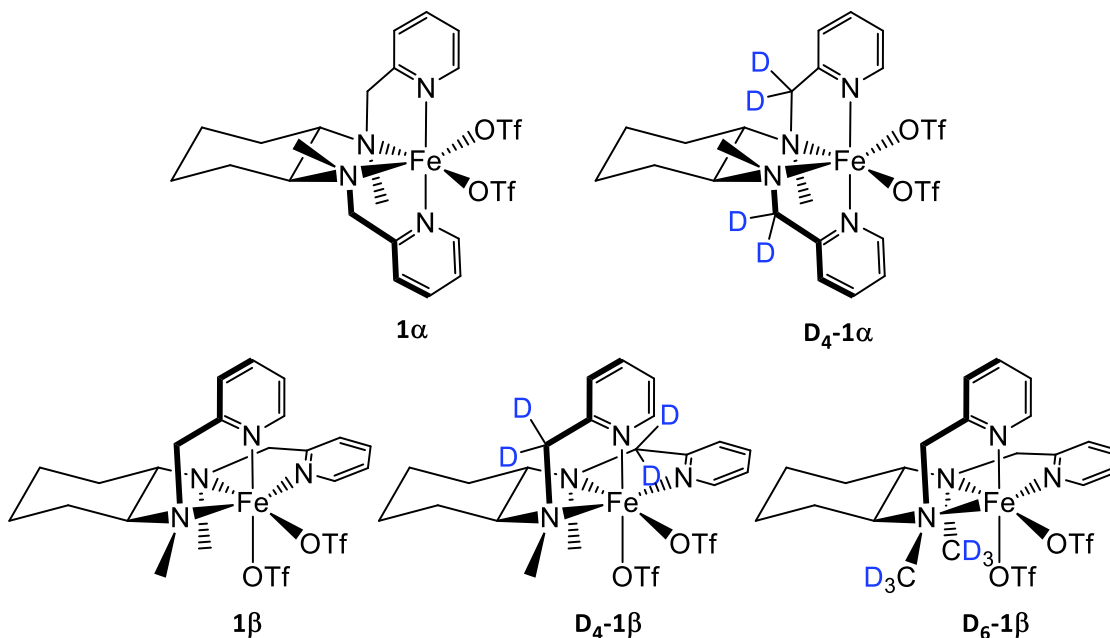
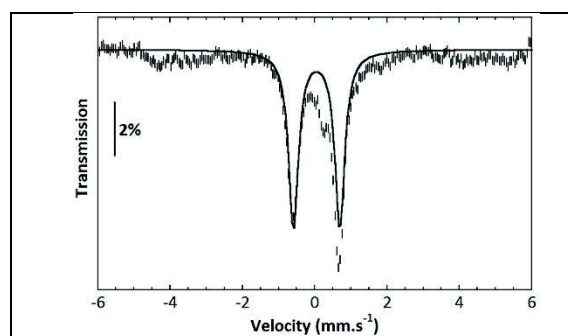


Figure 2. Iron complexes evaluated in this study.

RESULTS

Spectroscopic characterization of Fe^{IV}O species in catalytic oxidations. The pair of complexes **1 α** and **1 β** catalyze water oxidation using NaIO₄ or CAN as oxidant.¹⁶ High valent oxo-iron species α -[Fe^{IV}(O)(H₂O)(mcp)]²⁺ (**2 α**) and β -[Fe^{IV}(O)(H₂O)(mcp)]²⁺ (**2 β**) are proposed to be the resting state in these reactions on the basis of their distinctive UV-Vis spectra ($\lambda_{\text{max}} = 769 \text{ nm}$, $\epsilon = 270 \text{ M}^{-1} \text{ cm}^{-1}$ for **2 α** ; $\lambda_{\text{max}} = 778 \text{ nm}$, $\epsilon = 280 \text{ M}^{-1} \text{ cm}^{-1}$ for **2 β**), ESI-MS spectra ($m/z = 413.162 \pm 0.003$ assigned to [Fe^{IV}(O)(OH)(mcp)]⁺, in H₂¹⁸O and D₂O a +4 and a +1 shifts observed, respectively) and by resonance Raman in the case of **2 α** ($\lambda_{\text{exc}} = 413.1 \text{ nm}$, 822 cm^{-1} , downshifted by 40 cm^{-1} with the use of H₂¹⁸O).¹⁶ However, a Mössbauer analyses that could unambiguously prove the high oxidation state nature of the iron center could not be obtained. We note in passing that high valent iron oxo species are also considered as the water oxidizing agents in several coordination complexes, including mononuclear and polynuclear examples, but in none of these cases has Mössbauer evidence been obtained.^{16-22,24,29,33,37,40-45} Interestingly, spectroscopic

evidence has been built supporting the implication of high valent iron oxo species in water oxidation reactions by iron containing materials such as hematites and oxo(hydroxide)NiFe oxides.^{46,47} Notably, Mössbauer characterization of a Fe^{IV} intermediate has been recently obtained in operando analysis of NiFe and Fe oxyhydroxide electrocatalysts.⁴⁸ Frozen solutions of putative **2α** and **2β**, stored under liquid N₂ few days before Mössbauer analysis is conducted showed instead spectra characteristic of mononuclear ferric complexes (see SI section 8). Reasoning that the complexes may undergo slow degradation even in N₂-frozen solution, we generated **2α** and **2β** by reaction of **1α** and **1β** dissolved in (acidic) water with 1.2 equiv of NaIO₄, and the corresponding frozen solutions were immediately subjected to Mossbauer analysis. The corresponding Mössbauer spectra look very much alike (Figure 3) with a central doublet centered near $\delta = 0.0$ mm s⁻¹ flanked by contributions extending over a large velocity range (ca -8 to +8 mm s⁻¹). These spectra suggest the presence of a mixture of Fe^{IV} and Fe^{III} species, what was confirmed by experiments conducted at 4.5 K under weak (0.06 T) and strong (7 T) magnetic fields applied parallel to the γ -rays (Figure SI. 44). The latter spectra could be nicely simulated with hyperfine parameters classical for both type of species (Table SI.9).⁴⁹ In particular, the parameters obtained for the central doublets characterize **2α** and **2β** as *bona fide* S=1 Fe^{IV}=O species (Table SI.9). These complexes are not stable on the long run and decay rapidly to Fe^{III} species (Figure SI.43 and 44). In this respect it is worth noting that these Mössbauer data indicate that **2α** is significantly more stable than **2β**, as judged both from the higher amount of Fe^{IV} present in the original sample (ca 60 % for **2α** vs ca 40 % for **2β**) and its slower rate of the decay (Figure SI.43 and 44).



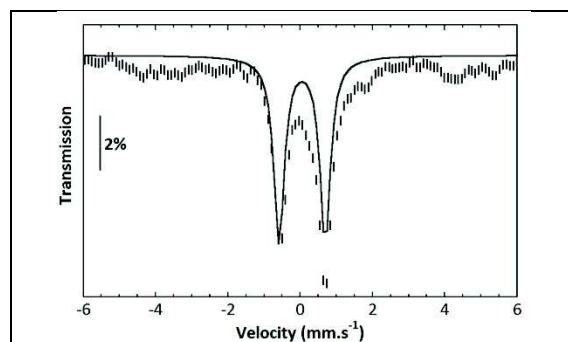
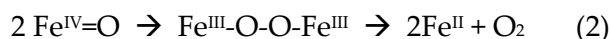


Figure 3. Mössbauer spectra of **2α** (top) and **2β** (bottom) at 80 K hatched bars: experimental spectrum; solid line simulation with the parameters given in Table SI.8. Selected parameters; **2α**; $\delta = 0.04 \text{ mm}\cdot\text{s}^{-1}$, $\Delta E_Q = 1.28 \text{ mm s}^{-1}$, $\Gamma = 0.20$, $\eta = 0.43$, $A_x = -29.5$, $A_y = -16.3$, $A_z = -9.5$. **2β**; $\delta = 0.04 \text{ mm}\cdot\text{s}^{-1}$, $\Delta E_Q = 1.28 \text{ mm s}^{-1}$, $\Gamma = 0.15$, $\eta = 0.86$, $A_x = -25.5$, $A_y = -13.7$, $A_z = -8.5$.

Formation and decay of oxoiron(IV) species under slight excess of oxidant. It has been previously described that water oxidation by **1α** and **1β** with chemical oxidants is sustained as long as the putative $\text{Fe}^{\text{IV}}(\text{O})\text{L}^{\text{N}4}$ species (where $\text{L}^{\text{N}4}$ is a tetradentate aminopyridyl ligand such as mcp), considered to be the resting state on the basis of UV-vis and ESI-MS monitoring, are present in the reaction mixture.¹⁶⁻¹⁸ The Mössbauer characterization of **2α** and **2β** provides strong reliability to this proposal. Thus, decomposition of $\text{Fe}^{\text{IV}}(\text{O})\text{L}^{\text{N}4}$ is linked with depletion of catalytic activity. It can therefore be considered that identification of the decay paths of **2α** and **2β** will be useful in designing more robust catalysts.

Towards this end, decay of **2α** and **2β** under aqueous acidic conditions of relevance to catalytic water oxidations were first analyzed. **2α** (1 mM, pH = 1, 25 °C) was generated by oxidizing **1α** with CAN (2.5-3 eq.). The intermediate, generated following this procedure, proved to be unstable, as shown by UV-Vis spectroscopy, in particular by monitoring of the decay of the characteristic NIR band of the complex (Figure 4a, $\lambda = 769 \text{ nm}$, $\epsilon = 270 \text{ M}^{-1}\text{cm}^{-1}$, $t_{1/2} = 0.15 \text{ h}$). Under the same conditions, the oxidation of **1β** produces **2β**, characterized by a lower energy d-d band ($\lambda = 778 \text{ nm}$, $\epsilon = 280 \text{ M}^{-1}\text{cm}^{-1}$). Noticeable, **2β** exhibits a shorter half-life than **1α** ($t_{1/2} = 0.11 \text{ h}$, see figure SI.22).

After complete decay of **2α** and **2β**, no traces of O₂, or CO₂ (in the gas phase, measured by GC-TCD and manometry) or H₂O₂ (in solution, measured by titration with the peroxotitanyl method)⁵⁰ were detected. Hence we can discard that the decay of **2α** and **2β** involves; a) reaction of **2α** and **2β** with H₂O to form the O-O bond (reaction 1), and b) O-O bond formation by interaction of two units of Fe^{IV}=O (reaction 2).



ESI-HRMS analyses of the reaction mixtures formed after decay of **2α** (Figure 4b) display major ion peaks corresponding to mononuclear Fe^{III} species (in deuterated water solution, [Fe^{III}(OD)₂(mcp)]⁺, m/z = 416.1848; [Fe^{III}(OD)(CF₃SO₃)(mcp)]⁺, m/z = 547.1278; [Fe^{III}(OD)(mcp)]²⁺, m/z = 199.0891) together with partial ligand fragmentation ([mcp+O-2H]+D]⁺, m/z = 340.225 and [mcp-CH₂py+2D]⁺, m/z = 236.210).

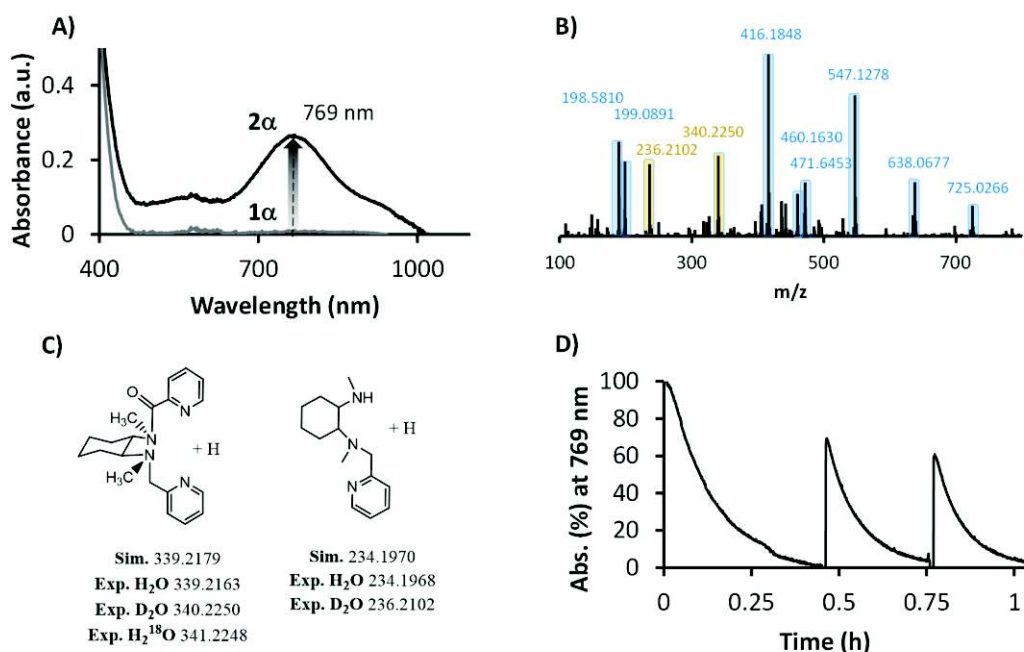


Figure 4. A) UV-Vis spectrum of **2α** (black) in water formed by reaction of **1α** (gray) (1 mM) with 3 eq. of CAN in HOTf (final pH = 1, 25 °C) and B) ESI-HRMS recorded 1.5 hour after of the addition of CAN (3 eq., 50 μL) to **1α** (4.5 mM, 0.5 mL) in D₂O. Blue peaks correspond to iron species while brown peaks correspond to ligand fragments. C)

Ligand fragmentation observed by CSI-HRMS in reactions performed in H₂O, D₂O and H₂¹⁸O. D) Evolution of the **2α** chromophore monitored at 769 nm after the addition of 1 eq. of CAN (x 3 times).

The observation that ferric species with the intact ligand dominate the spectra suggests that **2α** may be regenerated upon further oxidation. Indeed, after its full decay (ca. 0.8 h, judged by UV-Vis, Figure 4d), **2α** could be recovered up to 70% (according to the intensity of the $\lambda = 769$ nm band) by adding just one equivalent of CAN. The same procedure applied to **2β** revealed that only 50% of the oxo-Fe(IV) intermediate could be reformed by addition of one equivalent of CAN (see SI section 4). Thus, **2β** decays and irreversibly decomposes faster than **2α**.

Following decay of **2β** and **2α**, reaction mixtures were treated with NaOH to induce complete demetalation. Subsequent extraction with an organic solvent permitted to isolate the ligand and organic products arising from its oxidative degradation. Interestingly, ESI-MS analysis of the extracted mixtures (Figure 5), revealed that the major ligand oxidation fragments obtained after the decay of **2α** and **2β** are different. In the case of **2α**, ligand fragments arise from the breakage of the pyridylmethyl arm presumably initiated through oxidation of the benzylic methylene site (339.21 ([C₂₀H₂₆N₄O]+H⁺) and 234.19 m/z ([C₁₄H₂₃N₃]+H⁺) assigned to [**mcp(+O-2H)**]+H⁺ and [**mcp-CH₂Py+H**]+H⁺, respectively, depicted in Figure 5a). Instead, the main peak observed after decay of **2β** (Figure 5b) results from the loss of a methyl group, presumably through oxidation of the N-methyl position (311.22 m/z ([C₁₉H₂₆N₄]+H⁺) assigned to [**mcp(-Me+H)**]+H⁺, depicted in Figure 4c). Oxygenation of a methylenic site (m/z = 339.21) is also observed as a minor path. Thus, this analysis suggests that **2β** and **2α** decay *via* different paths. Since **2α** and **2β** are topological isomers, it can be concluded that the particular tridimensional arrangement of the ligand in these coordination complexes define specific decay paths.

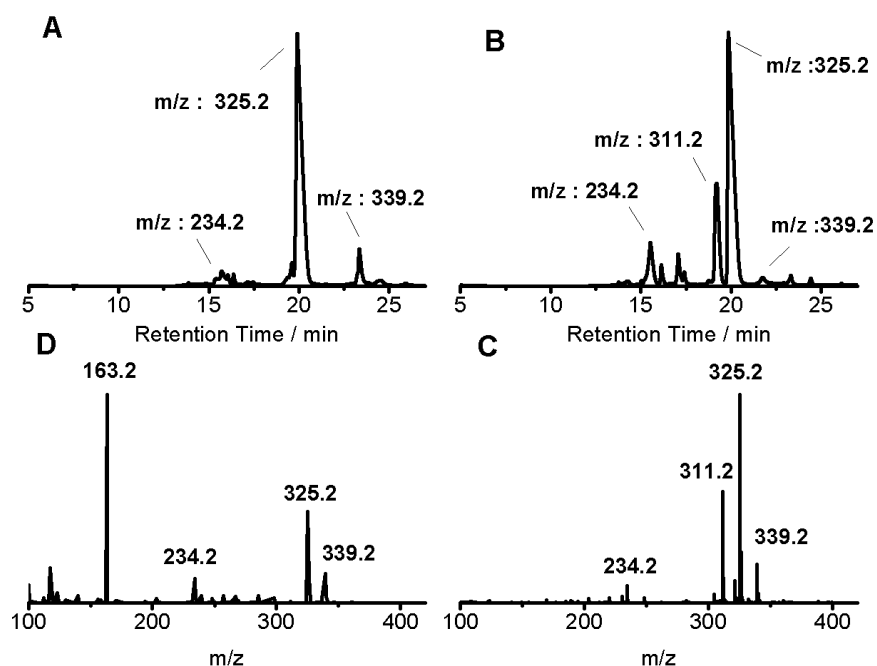


Figure 5. Top: HPLC chromatograms of the extracted ligand fragments after complete decay and demetalation of oxoiron(IV) complexes **2 α** (panel A) and **2 β** (panel B), see supporting information for details of the ligand extraction procedures. **2 α** and **2 β** were generated by reacting **1 α** or **1 β** (1 mM) with CAN (3 mM). The absorbance detection was performed at 247 nm, coinciding with the maximum absorption of the pyridine chromophore. Bottom: HRMS spectra of the extracted decay mixture of **1 α** or **1 β** (1 mM, respectively **panels C** and **D**) with CAN (3 mM) recorded in CHCl₃ at 298 K. The observed peaks can be assigned to ligand oxidation fragments, as follow: m/z: 234.2 fragment [mcp-CH₂Py]H⁺ (chemical formula: C₁₄H₂₄N₃); m/z: 163.2 fragment [mcp]2H⁺ (chemical formula: C₂₀H₃₀N₄); m/z: 325.2 fragment [mcp]H⁺ (chemical formula: C₂₀H₂₉N₄); m/z: 311.2 fragment [mcp-Me]H⁺ (chemical formula: C₁₉H₂₇N₄) and m/z: 339.2 fragment [mcp+O]H⁺ (chemical formula: C₂₀H₂₇N₄O).

The identification of the oxidized fragment structures was unambiguously corroborated by performing HPLC-MS analyses of the extracted decay mixtures (Figures 4, 5 and S.I. Section 5), and by comparison of the HPLC-MS retention times with

independently prepared samples of the presumed fragments. Moreover, the quantification of the fragments contained in the extracted residues was also performed by HPLC-MS (Figure 6). Blank experiments, applied to aqueous solutions of **1 α** and **1 β** , show that ~90% of the ligand is recovered by this procedure. This analysis thus provides a detailed picture of the fate of the ligand, which in turn can be satisfactorily correlated with the decay paths of the catalysts.

In first place, HPLC-MS analyses of the extracted mixtures obtained after the initial decay of **2 α** and **2 β** showed that the amount of intact ligand (mcp) is in good agreement with the percentage of oxoiron(IV) species that can be regenerated upon a second addition of oxidant (69% and 50% for **1 α** and **1 β** , respectively). This observation strongly suggests that irreversible decay of **2 α** and **2 β** does not entail a hydrolytic/demetallation process, without ligand oxidation. In other words, the ligand remains ligated to the iron center and free ligand never accumulates in solution, despite of the highly acidic conditions of the reactions mixtures. The high stability of **2 α** under acidic conditions is especially notable when compared with its ferrous precursor **1 α** .³⁶ This contrasting behavior can be understood by considering the respective labile and inert character of the high spin (S=2) Fe(II) and low spin (S=1) Fe(IV) complexes. Indeed, oxo-iron(IV) complexes with aminopyridine ligands are known to be remarkably stable under highly acidic conditions.⁵¹⁻⁵³

In second place, the oxidative demethylation of a NMe group is confirmed to be the main decomposition pathway associated to **2 β** ; in fact, the decay mixture shows that 20% of the ligand has been converted into the **mcp-Me** fragment ([C₁₉H₂₆N₄], figure 6). The degradation of the mcp ligand, upon decay of **2 β** , also occurs through oxidation at the benzylic methylenic sites, however, in a relatively minor extent (< 10%). Instead, the demethylation pathway seems to be hampered for **2 α** . Only traces of the **mcp-Me** fragment could be detected. The major fragments obtained from the degradation of **2 α** can be rationalized to originate from the initial oxidation of the benzylic methylenic sites.

Formation and decay under excess of oxidant. When the same analysis is performed after the reaction of **1 α** and **1 β** with 75 mM of Ce^{IV}, conditions that are catalytically relevant for water oxidation,¹⁸ ligand oxidative degradation is evidenced to be more

important (Figure 6). Importantly, the nature of the fragments observed after the water oxidation reaction, are in good agreement with the products obtained after decomposition of **2 α** ; about 60% of the entire **mcp** ligand was still recovered at the end of the reaction (judged by HPLC-MS). However, reaction of **1 β** leads to the almost complete decomposition of the **mcp** ligand, and identifiable fragments account only for roughly 30-35% of the original amount of ligand. In addition, multiple minor products, presumably ligand fragments formed by multiple oxidative degradation, are observed (Figure 6).

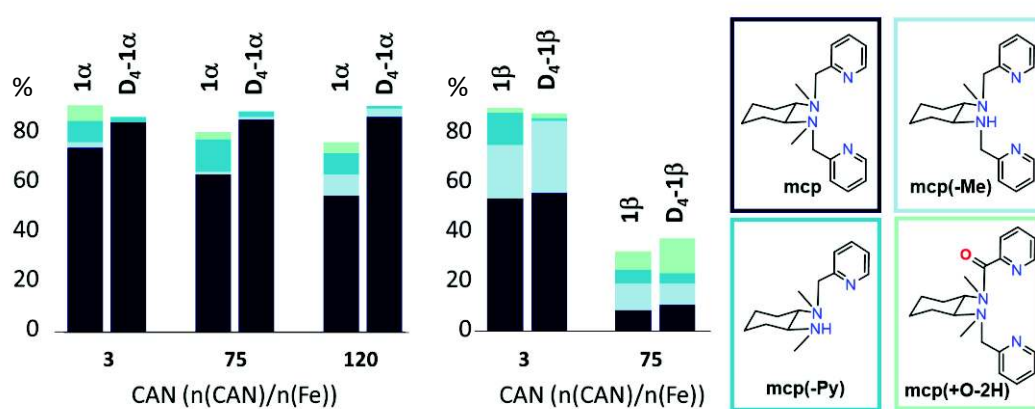


Figure 6. Quantification of the ligand degradation products (in % respect to the theoretical amount) after reaction of **1 β** , **D₄-1 β** (1 mM) in water with CAN (3, 75 or 100 mM), demetalation and ligand extraction. Ligand fragments were identified by HPLC-MS and by comparison with independently prepared products. See experimental for details.

Deuteration. Ligand degradation analyses described above indicate that the pseudobenzyl methylenic C-H bonds of the **mcp** ligand are the most prone sites for the oxidative degradation of **1 α** and derived species under stoichiometric and catalytic conditions. This led us considering possible strategies for protecting/strengthening these positions. We rationalized that provided the catalyst has a molecular nature, deuteration of these sites will provide stronger C-H bonds, while retaining the electronic and structural properties of the catalyst intact, and therefore the lifetime of the catalyst

will be extended. Following on this reasoning, tetradeutero **D₄-mcp** ligand was prepared by reacting **mcp** with NaH in CD₃CN, and the corresponding complexes α -D₄-[Fe^{II}(CF₃SO₃)₂(mcp)], **D₄-1 α** , and β -D₄-[Fe^{II}(CF₃SO₃)₂(mcp)], **D₄-1 β** , were prepared. Characterization of **D₄-1 α** and **D₄-1 β** , and in particular deuteration of the benzylic sites was confirmed by ¹H-NMR spectroscopy and MS analysis (See S.I. Section 3).

Effect of deuteration in the stability of D₄-2 α and in the catalytic water oxidation activity. Most gratifyingly, the simple deuteration of the pseudo-benzylic CH₂ sites in **1 α** has a very important impact in its catalytic activity, and in the stability of **D₄-2 α** . First of all, the half-life time of **D₄-2 α** , generated by addition of CAN (3 mM) to a water solution of **D₄-1 α** (1 mM), was enhanced 18-fold (monitored by UV-Vis spectroscopy) (Figure SI.20-21), from 0.15 h to 2.8 h with regard to its protio analogue. However, the deuteration of the pseudobenzylic positions does not modify the stability of **D₄-2 β** , which retains the same half-life of **2 β** (Figure SI.22-23).

Furthermore, following decay of **D₄-2 α** and **D₄-2 β** , the decay mixtures were subjected to the standard demetalation-extraction procedures, and ligand fragments analyzed (Figure 6). In the case of **D₄-2 α** , the minor degradation pathway associated with the oxidation of pseudo-benzylic CH₂ sites (producing **mcp(-Py)**, **mcp(+O-2H)**) appears to be further hampered by deuteration of these positions, and the recovery of the intact ligand increases from 69% (**2 α**) to 79% (**D₄-2 α**). Decay of **D₄-2 β** shows a different pattern. The percentage of unmodified ligand (**mcp**) does not change upon deuteration, but the relative amounts of products resulting from either the loss of a methylpyridine arm (**mcp(-Py)**) or a methyl group (**mcp(-Me)**) change, with the later increasing at the expenses of the former upon deuteration. This observation suggests that there is a competition between the paths leading to the two products. Deuteration does not improve the recovery of the ligand in reactions of **D₄-1 β** with excess CAN (75 mM), but instead it has a favorable positive effect in **1 α** , which is further retained when 120 mM CAN is employed (Figure 6, Table S.I.7). In all cases, deuteration leads to almost quantitative recovery of the intact ligand (~85%), demonstrating that ligand degradation

and demetalation for this catalyst is basically ligated to oxidation of this site, and most remarkably, the process is blocked by deuteration.

Manometry and GC-MS on-line studies of the gases evolved in the chemically driven WO. Catalytic activity of the series of complexes, including protio and deuterio analogues was studied in parallel in order to ensure proper comparison among the series. O₂ produced in the reactions was monitored by manometry and also by gas chromatography. Values determined by the two methods are in good agreement. For example, under catalytic conditions, manometric measurements indicate that **1α** and **D₄-1α** yield 379 ± 3 and 1732 ± 90 TON O₂, respectively (Table 1), values that are in good agreement with the values determined by GC (403 ± 10 and 1896 ± 110).^{16,18} Indeed, for the whole series of complexes, GC-TCD analyses of the gas at the headspace of the reactions confirmed that the gas formed is essentially O₂ (Table 1).

Most remarkably, these values indicate that deuteration creates a much more active catalyst, yielding approximately a fourfold increase in TONs. The O₂ produced for **D₆-β-Fe(OTf)₂(mcp) (D₆-1β)** (161 ± 2 TON O₂) is also roughly fourfold increased with respect to **D₄-β-Fe(OTf)₂(mcp) (D₄-1β)** and **β-Fe(OTf)₂(mcp) (1β)** (39 and 30 TON O₂, respectively), although absolute numbers are still modest when compared with **1α** and **D₄-1α**. The improved performance of **D₆-1β** can be rationalized taking into account the previous analysis of decay paths, which indicated substantial degradation of this isomer *via* oxidation of the *N*-methyl groups. Accordingly, deuteration of these groups in **D₆-1β** prevents its decomposition and allows for a more sustained oxygen evolution activity. None of the complexes shows induction time in their catalytic activity. In addition, it is particularly noticeable that **D₄-1α** and **1α** have the same initial rate for oxygen evolution (See Figure 8 a, b). This has important mechanistic implications since the metal center in both **D₄-1α** and **1α** complexes experience the same electronic and steric properties. Equivalent O₂ evolution rates strongly evidences catalytic species only differing on the isotopic nature of the pseudobenzyl positions. Iron complexes containing as ligands different degradation fragments of the mcp ligand (See Figure 7) were prepared and their activity as water oxidation catalysts was tested. These complexes do not show

appreciable water oxidation catalytic activity. In addition, iron complexes where the methyl groups of the mcp ligand are replaced by protons or with the two pyridyl positions oxidized are also catalytically incompetent.⁵⁴ Therefore, the initial O₂ evolution should come from the intact species before degradation. Altogether strongly indicates the molecularity of the catalytic system and that the original molecular complex is the active species. The same trend was observed for the pair **1β** and **D₄-1β** but they are somewhat different for **D₆-1β**. Presumably, initial rates measured for **1β** and **D₄-1β** are already contaminated by rapid catalyst degradation (Table 1 entries 8-10 and Figure 8 and SI.45).

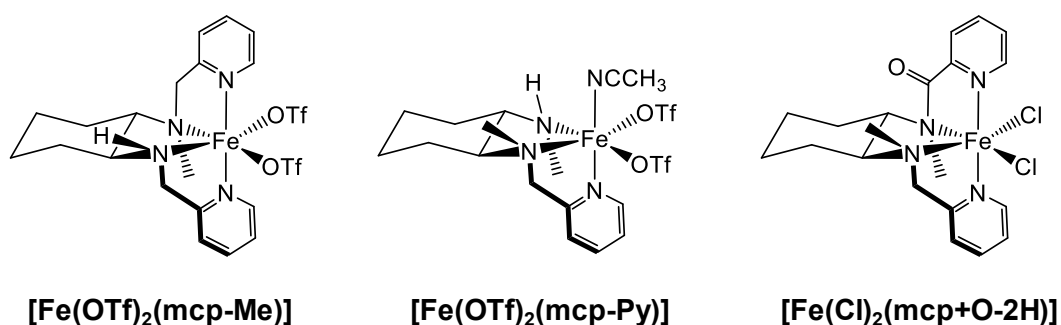


Figure 7. Iron complexes of the fragmented ligands, tested under standard water oxidation catalysis conditions.

Table 1. Water oxidation catalytic activities for the studied iron complexes.

Entry	Complex	[CAN] (Mm)	[Cat] (μm)	TOF (h ⁻¹) ^a	TON O ₂ ^a	TON O ₂ ^b	Yield O ₂ (%)	TON CO ₂ ^b
1	1αFe^c	125	12.5	850	379 ± 3	403 ± 10	16 %	<1
2	D₄-1αFe^c	125	12.5	820	1732 ± 90	1896 ± 110	76 %	<1
3	1βFe^c	125	12.5	33	30 ± 1	46 ± 1	2 %	<1
4	D₄-1βFe^c	125	12.5	37	39 ± 2	52 ± 3	2 %	<1
5	D₆-1βFe^c	125	12.5	214	161 ± 2	151 ± 2	6 %	<1
6	mcp-Me^c	125	12.5	-	0	<1		<1
7	mcp-Py^c	125	12.5	-	0	<1		<1
8	1αFe^d	75	1000	150	12	-	64 %	-
9	D₄-1αFe^d	75	1000	200	17	-	91 %	-
10	1βFe^d	75	1000	74	9	-	48 %	-

Reactions performed in MilliQ water at 25 °C under vigorously stirring. a) Results obtained by manometry studies after 20 h of reaction. TOF is calculated after 5 min of

the addition of the catalyst. b) Results from the analysis of an aliquot of the head-space by GC-TCD after 20 h of reaction. c) Reaction conditions A: The catalyst (0.5 ml, final concentration 12.5 μM) was injected through a septum into the reaction vial containing CAN aqueous solution (9.5 ml, 131 mM, final concentration 125 mM). Initial pH is 0.8. d) Reaction conditions B: CAN (0.8 ml of stock solution in HOTf:H₂O 3:10 solution, final concentration 75 mM) was injected through a septum into the reaction vial containing the catalyst aqueous solution (3.2 ml, final concentration 1 mM) pH is 1. TOF is calculated after 1 min of the addition of the catalyst

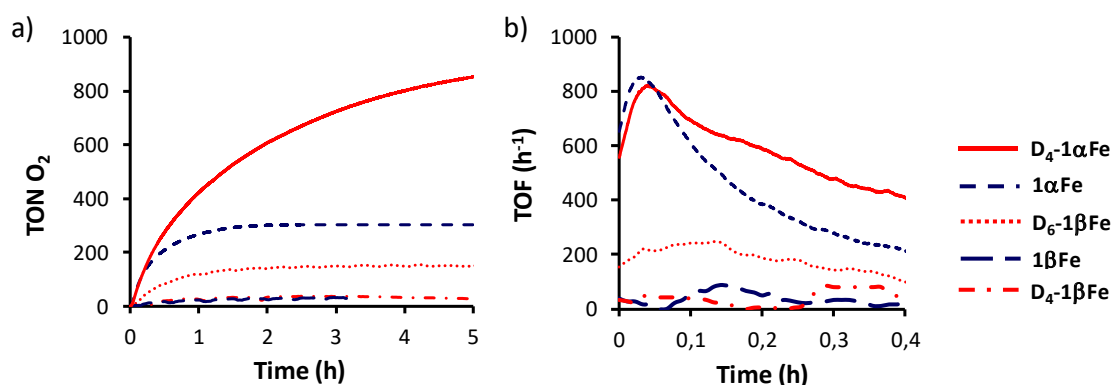


Figure 8. a) Gas traces and b) initial TOF (h⁻¹) of the manometry monitorization when the iron catalyst (α -Fe(OTf)₂(mcp) (short-dashed line), D₄- α -Fe(OTf)₂(mcp) (straight line), β -Fe(OTf)₂(mcp) (long-dashed line), D₄- β -Fe(OTf)₂(mcp) (dotted-short-dashed line) and D₆- β -Fe(OTf)₂(mcp) (dotted line)) (0.5 ml of a stock solution, final concentration 12.5 μM) is added to a stirred solution of CAN (9.5 ml, final concentration 1000 equiv., 125 mM) in Milli-Q water at 25°C and initial pH 0.8.

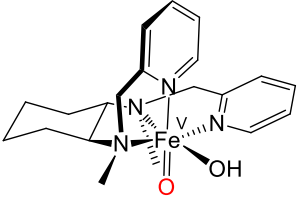
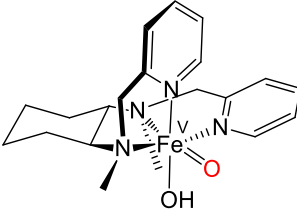
Direct GC-MS online-analysis of the gases evolved at the head-space along the reaction time permits to identify relative rates for O₂ and CO₂ evolution from the very beginning of the reaction to hundreds of seconds. In all cases the rates for O₂ evolution are much higher than the one measured for CO₂ production, being the latter only produced in trace levels. Thus, the measured reaction rates by manometry experiments are ascribed only to O₂ evolution. Likewise, catalyst decomposition is not connected with O₂ evolution. The sum of these results indicates that the higher activity of D₄-1 α results from a more robust character. In combination with the HPLC analysis of the degradation

paths, we can conclude that deuteration of the pseudobenzyl positions blocks the most important deactivation path, conferring stability to the catalyst.

Multiple oxidant addition experiments. The increase in TON (about 5 fold) obtained with **D₄-1 α** with respect to **1 α** nicely translates into substantially better yields of O₂ produced (76% *vs* 16%). However, this 5-fold increase appears modest when comparing the 18-fold improvement in the half-life time of **D₄-2 α** in comparison with **2 α** . Furthermore, while significant catalyst degradation is observed for **1 α** , ligand recovery experiments showed minimum degradation of **D₄-1 α** . This data let us to consider that the end of catalytic activity observed in **D₄-1 α** does not respond to a catalyst degradation process. Further optimization by lowering the catalyst concentration to 6.25 μ M yields a TON of 2800 (58 % yield), which is about one order of magnitude higher than previously reported values with **1 α** . These observations indicate that catalytic activity, at 12.5 μ M, with the most robust catalyst of the series (**D₄-1 α**) stops not as a result of catalyst degradation, but instead because of Nernstian effects in the Ce(IV)/Ce(III) potential. Considering the ratio of [Ce^{IV}]/[Ce^{III}] at which O₂ evolution stops after the first addition of CAN, we can determine a potential threshold of 1.62 V *vs* NHE for catalytic activity. The same value was consistently obtained when reactions were initiated with different amounts of CAN. Noticeable, this value is in reasonable agreement with the DFT computed value (1.73 V *vs* NHE) for the PCET from [Fe^{IV}(O)(OH₂)(mep)]²⁺ to [Fe^V(O)(OH)(mep)]²⁺ (mep = *N,N'*-bis(2-pyridylmethyl)-*N,N''*-dimethyl-1,2-diaminoethane),³⁷ suggesting that access to the active Fe^V(O)(OH) oxidant becomes unfavorable at this [Ce^{IV}]/[Ce^{III}] ratio.

DFT modelling of the decomposition pathways. DFT calculations have been conducted to evaluate the feasibility of the methylene/methyl oxidation mechanism by **1 α** and **1 β** topological isomers (see Computational details SI section 10). The geometry of the early proposed Fe^V(O)(OH) WO active species, **3** was first optimized for the two topological isomers (See computational details SI. Section 10). In the case of **3 β** complex, two *cis*-tautomers may exist in which the Fe^V=O moiety is parallel (**3 β -a**) or perpendicular (**3 β -b**) to the methyl groups of the mcp ligand (Table 2). According to the free energy differences between the β isomers, the intermediate **3 β -a** in the S = 3/2 ground spin state is the most stable form. Thus, **3 β -a** was chosen to carry out the mechanistic study.

Table 2: Spin states relative free energies (kcal·mol⁻¹) of the Fe^V(O)(OH) intermediates for complex **1β** in the two *cis*-tautomers **3β-a** and **3β-b**.

		
	3β-a	3β-b
S = 1/2	13.0	15.6
S = 3/2	0.0 ^a	2.7

[a] Free energies respect to the most stable structure.

The methyl groups in **3β-a** are close to the oxo moiety (See Fig. 9a). Therefore, it is expected that the decomposition of the **mcp** ligand may start with the oxidation of a CH₃ group. Indeed, the Fe^V=O in the quartet spin state surface directly hydroxylates the CH₃ group with a free energy barrier of 18.7 kcal·mol⁻¹ with respect to β-[Fe^V(O)(OH)(mcp)]²⁺ (**3β-a**) species, which can be reached under catalytic conditions.⁵⁵ (See SI. computational section for details) This result is in agreement with the experimentally observed methyl decomposition product. Finally, the free energy profile for the O-O bond formation was also computed to determine if the decomposition reaction pathway prevails in solution (Figure 9). The water nucleophilic attack on the Fe^V=O moiety follows an stepwise mechanism, as has been described previously,⁵ and the O-O bond formation event presents the highest in energy transition state (ΔG[‡] = 18.9 kcal·mol⁻¹; Figure 9). The methyl oxidation barrier is only 1.2 kcal·mol⁻¹ lower than the O-O bond formation one. These results suggest that the oxidation of the ligand may compete with the O-O bond formation event, providing a rational explanation for the origin of the reduced WO activity of **3β-a**.

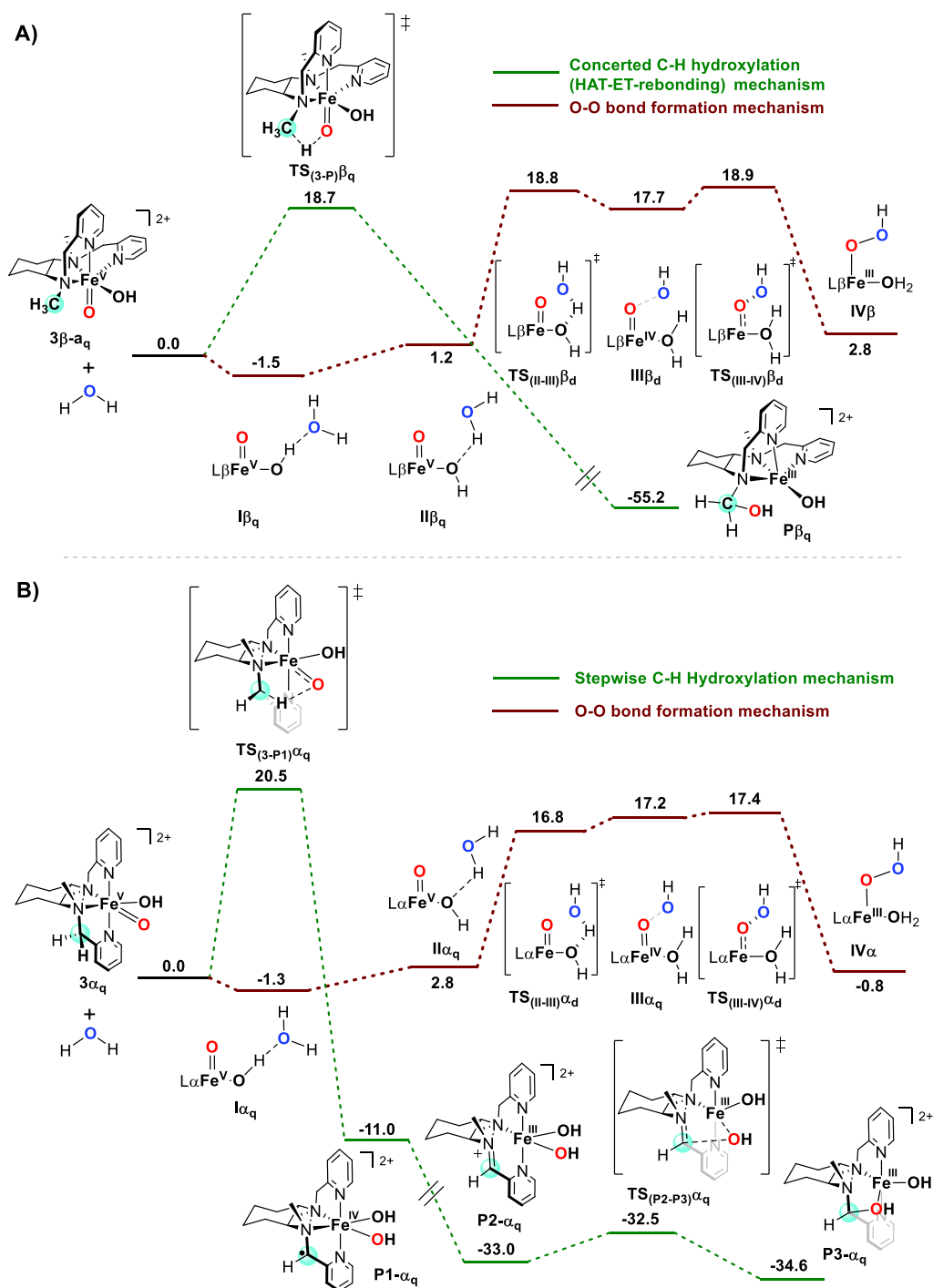


Figure 9. A) Comparison between the O-O bond formation and methyl oxidation mechanisms for $3\beta\mathbf{a}$. B) Comparison between the O-O bond formation and methylene oxidation mechanisms for 3α . Gibbs energies are in kcal·mol⁻¹. L stands for the mcp ligand.

For comparison reasons, the same calculations were performed also for 3α (Figure 9B). In this case, the methylene position is easier to oxidize ($\Delta G^\ddagger = 20.5$ kcal·mol⁻¹) than

the methyl group ($\Delta G^\ddagger = 25.6 \text{ kcal}\cdot\text{mol}^{-1}$, see Figure SI.49). This result is consistent with the methylene oxidation product detected by kinetic and ESI-MS experiments. Most remarkably, in contrast with **3 β a**, the transition state for the oxidation of the methylene is $3.5 \text{ kcal}\cdot\text{mol}^{-1}$ higher than the barrier for the O-O bond formation event.

Therefore, the computational analyses indicate that electrophilic attack of the $\text{Fe}^{\text{V}}(\text{O})$ species over the water molecule, leading to water oxidation is favored over ligand degradation via hydrogen atom transfer from the benzylic C-H bond in **3 α** . Instead, HAT from the N-Me group effectively competes with O-O bond formation in **3 β -a**. This analysis has obvious consequences that are in line with the experimental observations; a) in first place, **1 α** is a more robust WOC than **1 β** . b) Second, deuteration of the benzylic positions in **1 α** protects its more sensitive site for ligand oxidation. Owing to the stronger nature of the C-D over the C-H bond, ligand degradation becomes energetically more demanding. c) the most favorable site for ligand degradation in **1 β** is the NMe groups, and consistently, their deuteration limits the oxidative degradation, and enhances its catalytic activity. Deuteration of the pseudobenzylic methylenes in this case does not have a positive effect because these positions are not the most favorable oxidizable sites.

CONCLUSIONS

In this work the deactivation paths for iron water oxidation catalysts **1 α** and **1 β** have been studied. High valent oxoiron(IV) complexes **2 α** and **2 β** have been spectroscopically characterized, providing for the first time Mössbauer evidence for the implication of a high valent iron species in water oxidation reactions with homogeneous catalysts. **2 α** and **2 β** have been shown to degrade via processes that entail C-H oxidation of specific positions of the ligand. Interestingly, the locus of C-H oxidation is dependent on the nature of the catalyst, strongly suggesting that this is an intramolecular process, governed by the particular structure of the catalyst. Identification of the deactivation sites has been employed in the design of more robust catalysts by means of the deuteration of the ligand sensitive sites.

Of particular interest deuteration of the benzylic methylenic positions at **1 α** leads to the preparation of **D₄-1 α** , which is an extraordinarily robust and active catalysts.

Deuteration does not affect the water oxidation reaction rate nor the electronic nature of the catalyst, but the deuterated complex is oxidatively more robust, maintaining catalytic activity longer, and translating into larger TON (up to 1896 TON O₂). In addition, the lack of induction time in the O₂ evolution studies, and the much higher rate for O₂ evolution than for CO₂ production at the beginning of the reaction strongly suggest that the catalytically active species is molecular. Under specific conditions, using the most robust **D₄-1 α** complex, catalytic activity stops not because of catalyst degradation, but instead because of Nernst effects in the red-ox potential of the Ce^{IV}/Ce^{III} couple, setting a lower potential of 1.62 V for the generation of the water oxidation species with this catalyst. Of interest, this value is in agreement with the one determined for the proton transfer electron transfer oxidation of [Fe^{IV}(mep)(O)(OH₂)]²⁺ to [Fe^V(mep)(O)(OH)]²⁺.³⁷ TON > 2700 are obtained with **D₄-1Fe**, which represent the largest numbers obtained for a first row transition metal complex, and that are bypassed by only few examples of precious metal based catalysts.

Identification of structural weaknesses at molecular scale and its rational prevention provide proof beyond reasonable doubt of the molecular nature of this catalyst, converting the system in a privileged platform for studying O-O bond lysis/formation reactions of relevance to biology.

ASSOCIATED CONTENT

Supporting information

Sample preparation details and spectroscopic and spectrometric characterization; spectral simulations of Mössbauer analyses, computational details and coordinates.

AUTHOR INFORMATION

Corresponding authors

*jlloret@iciq.es

*miquel.costas@udg.edu

Notes

The authors declare no competing financial interests.

ACKNOWLEDGMENTS

We acknowledge the Spanish Ministry of Science CTQ2015-70795-P (M. C.), CTQ2016-80038-R (J. LL. F.), CTQ2014-59212-P (J. M. Lluís). We would like to thank the European Commission for the ERC-CG-2014-648304 (J.LL-F) project. The Spanish Ministry of Science is acknowledged for a FPU fellowship to C.C.. The financial support from ICIQ Foundation and CELLEX Foundation through the CELLEX-ICIQ Starting Career Program is gratefully acknowledged. This work has been partially supported by Labex ARCANÉ and CBH-EUR-GS (ANR-17-EURE-0003)

REFERENCES:

- (1) Blakemore, J. D.; Crabtree, R. H.; Brudvig, G. W. *Chem. Rev.* **2015**, *115*, 12974.
- (2) Karkas, M. D.; Verho, O.; Johnston, E. V.; Akermark, B. *Chem. Rev.* **2014**, *114*, 11863.
- (3) Meyer, T. J.; Sheridan, M. V.; Sherman, B. D. *Chem. Soc. Rev.* **2017**, *46*, 6148.
- (4) Blakemore, J. D.; Crabtree, R. H.; Brudvig, G. W. *Chem. Rev.* **2015**, *115*, 12974.
- (5) Stracke, J. J.; Finke, R. G. *ACS Catal.* **2014**, *4*, 909.
- (6) Fukuzumi, S.; Jung, J.; Yamada, Y.; Kojima, T.; Nam, W. *Chem. Asian J.* **2016**, *11*, 1138.
- (7) Crabtree, R. H. *Chem. Rev.* **2015**, *115*, 127.
- (8) Fukuzumi, S.; Hong, D. C. *Eur. J. Inorg. Chem.* **2014**, 645.
- (9) Li, J.; Guttinger, R.; More, R.; Song, F.; Wan, W.; Patzke, G. R. *Chem. Soc. Rev.* **2017**, *46*, 6124.

- (10) Wu, X.; Li, F.; Zhang, B.; Sun, L. *J. Photochem. and Photobiol. C: Photochem. Rev.* **2015**, *25*, 71.
- (11) Parent, A. R.; Sakai, K. *ChemSusChem* **2014**, *7*, 2070.
- (12) Hunter, B. M.; Gray, H. B.; Muller, A. M. *Chem. Rev.* **2016**, *116*, 14120.
- (13) Singh, A.; Spiccia, L. *Coord. Chem. Rev.* **2013**, *257*, 2607.
- (14) Najafpour, M. M.; Renger, G.; Holynska, M.; Moghaddam, A. N.; Aro, E. M.; Carpentier, R.; Nishihara, H.; Eaton-Rye, J. J.; Shen, J. R.; Allakhverdiev, S. I. *Chem. Rev.* **2016**, *116*, 2886.
- (15) Karkas, M. D.; Akermark, B. *Dalton Trans.* **2016**, *45*, 14421.
- (16) Codola, Z.; Gomez, L.; Kleespies, S. T.; Que, L., Jr.; Costas, M.; Lloret-Fillol, J. *Nat. Commun.* **2015**, *6*.
- (17) Codolà, Z.; Garcia-Bosch, I.; Acuña-Parés, F.; Prat, I.; Luis, J. M.; Costas, M.; Lloret-Fillol, J. *Chem. Eur. J.* **2013**, *19*, 8042.
- (18) Fillol, J. L.; Codolà, Z.; Garcia-Bosch, I.; Gómez, L.; Pla, J. J.; Costas, M. *Nat. chem.* **2011**, *3*, 807.
- (19) Tan Peng, K. H.-K. L. T.-C. *ChemComm* **2014**, *50*, 12779.
- (20) Chen, G.; Chen, L.; Ng, S. M.; Man, W. L.; Lau, T. C. *Angew. Chem. Int. Ed.* **2013**, *52*, 1789.
- (21) To, W.-P.; Wai-Shan Chow, T.; Tse, C.-W.; Guan, X.; Huang, J.-S.; Che, C.-M. *Chem. Sci.* **2015**, *6*, 5891.
- (22) Hong, D.; Mandal, S.; Yamada, Y.; Lee, Y. M.; Nam, W.; Llobet, A.; Fukuzumi, S. *Inorg. Chem.* **2013**, *52*, 9522.
- (23) Das, B.; Lee, B.-L.; Karlsson, E. A.; Akermark, T.; Shatskiy, A.; Demeshko, S.; Liao, R.-Z.; Laine, T. M.; Haukka, M.; Zeglio, E.; Abdel-Magied, A. F.; Siegbahn, P. E. M.; Meyer, F.; Karkas, M. D.; Johnston, E. V.; Nordlander, E.; Akermark, B. *Dalton Trans.* **2016**, *45*, 13289.
- (24) Wickramasinghe, L. D.; Zhou, R.; Zong, R.; Vo, P.; Gagnon, K. J.; Thummel, R. P. *J. Am. Chem. Soc.* **2015**, *137*, 13260.
- (25) Coggins, M. K.; Zhang, M.-t.; Vannucci, A. K.; Dares, C. J.; Meyer, J. *J. Am. Chem. Soc.* **2014**, *136*, 5531–5534.
- (26) Liu, Y.; Xiang, R.; Du, X.; Ding, Y.; Ma, B. *Chem. Commun.* **2014**, *50*, 12779.
- (27) Klepser, B. M.; Bartlett, B. M. *J. Am. Chem. Soc.* **2014**, *136*, 1694.
- (28) Panchbhai, G.; Singh, W. M.; Das, B.; Jane, R. T.; Thapper, A. *Eur. J. Inorg. Chem.* **2016**, *2016*, 3262.
- (29) Najafpour, M. M.; Safdari, R.; Ebrahimi, F.; Rafighi, P.; Bagheri, R. *Dalton Trans.* **2016**, *45*, 2618.
- (30) Annunziata, A.; Esposito, R.; Gatto, G.; Cucciolito, M. E.; Tuzi, A.; Macchioni, A.; Ruffo, F. *Eur. J. Inorg. Chem.* **2018**, *2018*, 3304.
- (31) Das, B.; Orthaber, A.; Ott, S.; Thapper, A. *ChemSusChem* **2016**, *9*, 1178.
- (32) Coggins, M. K.; Zhang, M.-T.; Vannucci, A. K.; Dares, C. J.; Meyer, T. J. *J. Am. Chem. Soc.* **2014**, *136*, 5531.
- (33) Kottrup, K. G.; Hettterscheid, D. G. H. *Chem. Commun.* **2016**, *52*, 2643.
- (34) Wang, Z.-Q.; Wang, Z.-C.; Zhan, S.; Ye, J.-S. *Appl. Catal., A* **2015**, *490*, 128.
- (35) Kottrup, K. G.; D'Agostini, S.; van Langevelde, P. H.; Siegler, M. A.; Hettterscheid, D. G. H. *ACS Catal.* **2018**, *8*, 1052.
- (36) Esarey, S. L.; Holland, J. C.; Bartlett, B. M. *Inorg. Chem.* **2016**, *55*, 11040.
- (37) Acuna-Pares, F.; Codola, Z.; Costas, M.; Luis, J. M.; Lloret-Fillol, J. *Chem. Eur. J.* **2014**, *20*, 5696.
- (38) Acuña-Parés, F.; Costas, M.; Luis, J. M.; Lloret-Fillol, J. *Inorg. Chem.* **2014**, *53*, 5474.
- (39) Sala, X.; Maji, S.; Bofill, R.; García-Antón, J.; Escriche, L.; Llobet, A. *Acc. Chem. Res.* **2014**, *47*.

- (40) Okamura, M.; Kondo, M.; Kuga, R.; Kurashige, Y.; Yanai, T.; Hayami, S.; Praneeth, V. K.; Yoshida, M.; Yoneda, K.; Kawata, S.; Masaoka, S. *Nature* **2016**, *530*, 465.
- (41) Staehle, R.; Tong, L. P.; Wang, L.; Duan, L. L.; Fischer, A.; Ahlquist, M. S. G.; Sun, L. C.; Rau, S. *Inorg. Chem.* **2014**, *53*, 1307.
- (42) Parent, A. R.; Nakazono, T.; Lin, S.; Utsunomiya, S.; Sakai, K. *Dalton Trans* **2014**, *43*, 12501.
- (43) Liao, R.-Z.; Li, X.-C.; Siegbahn, P. E. M. *Eur. J. Inorg. Chem.* **2014**, 728.
- (44) Ertem, M. Z.; Gagliardi, L.; Cramer, C. J. *Chem. Sci.* **2012**, *3*, 1293.
- (45) Ellis, W. C.; McDaniel, N. D.; Bernhard, S.; Collins, T. J. *J. Am. Chem. Soc.* **2010**, *132*, 10990.
- (46) Takashima, T.; Ishikawa, K.; Irie, H. *The J. of Phys. Chem. C* **2016**, *120*, 24827.
- (47) Zandi, O.; Hamann, T. W. *Nat Chem* **2016**, *8*, 778.
- (48) Chen, J. Y. C.; Dang, L.; Liang, H.; Bi, W.; Gerken, J. B.; Jin, S.; Alp, E. E.; Stahl, S. *S. J. Am. Chem. Soc.* **2015**, *137*, 15090.
- (49) McDonald, A. R.; Que, L., Jr. *Coord. Chem. Rev.* **2013**, *257*, 414.
- (50) Garcia-Bosch, I.; Company, A.; Frisch, J. R.; Torrent-Sucarrat, M.; Cardellach, M.; Gamba, I.; Guell, M.; Casella, L.; Que, L.; Ribas, X.; Luis, J. M.; Costas, M. *Angew Chem. Int. Ed.* **2010**, *49*, 2406.
- (51) Wang, D.; Ray, K.; Collins, M. J.; Farquhar, E. R.; Frisch, J. R.; Gomez, L.; Jackson, T. A.; Kerscher, M.; Waleska, A.; Comba, P.; Costas, M.; Que, L., Jr. *Chem. Sci.* **2013**, *4*, 282.
- (52) Garcia-Bosch, I.; Codolà, Z.; Prat, I.; Ribas, X.; Lloret-Fillol, J.; Costas, M. *Chem. Eur. J.* **2012**, *18*, 13269.
- (53) Park, J.; Lee, Y.-M.; Nam, W.; Fukuzumi, S. *J. Am. Chem. Soc.* **2013**, *135*, 5052.
- (54) Detz, R. J.; Abiri, Z.; Kluwer, A. M.; Reek, J. N. H. *ChemSusChem* **2015**, *8*, 3057.
- (55) Ha, E. H.; Ho, R. Y. N.; Kosiel, J. F.; Valentine, J. S. *Inorg. Chem.* **1995**, *34*, 2265.